Journal of Photochemistry and Photobiology A: Chemistry 216 (2010) 133–141

Contents lists available at ScienceDirect

Journal of Photochemistry and Photobiology A: Chemistry

journal homepage: www.elsevier.com/locate/jphotochem

# Controlled mesoporous self-assembly of ZnS microsphere for photocatalytic degradation of Methyl Orange dye

M. Muruganandham[a,*], R. Amutha[a], Evelina Repo[a], Mika Sillanpää[a,b], Yoshihumi Kusumoto[c], Md. Abdulla-Al-Mamun[c]

[a] University of Eastern Finland, Laboratory of Applied Environmental Chemistry, Patteristonkatu 1, Mikkeli 50100, Finland
[b] Faculty of Technology, Lappeenranta University of Technology, Patteristonkatu 1, FI-50100 Mikkeli, Finland
[c] Department of Chemistry and Bioscience, Graduate school of Science and Engineering, Kagoshima University, 1-21-35 Korimoto, Kagoshima 890-0065, Japan

ARTICLE INFO

*Article history:*
Available online 12 June 2010

*Keywords:*
ZnS
Photocatalysts
Mesoporous
Degradation
Methyl Orange

ABSTRACT

In this article, we have reported self-assembled synthesis of pore tunable, mesoporous ZnS microsphere and its photocatalytic activity. The photocatalytic activity was evaluated using Methyl Orange (MO) as model pollutant under UV light irradiation. The mesoporous photocatalysts was synthesized using hydrothermal method without using any templates or catalysts in large scale. The products were characterized by field emission scanning electron microscopy (FE-SEM), high resolution transmission electron microscopy (HR-TEM), X-ray diffraction (XRD) and energy-dispersive X-ray spectrometry (EDX). The nitrogen adsorption analysis confirmed the presence of mesoporous structure. The pore size of the photocatalysts could be enlarged from 2.6 to 7.2 nm by changing the concentration of the zinc precursor. The microsphere formation has been facilitated by self-assembly followed by Ostwald ripening process. In conclusion, this simple synthetic methodology open new vistas to prepare mesoporous photocatalysts in large scale.



## 1. Introduction

Synthesis and understanding the growth of nano/micro structured photocatalysts and study their applications are at the leading edge of today's research. Design and synthesis of well defined morphology and surface properties-controlled colloidal nanocrystals have been intensively studied in the past decade for their size and shape-dependent properties [1,2]. A simple, template free self-assemble process may provide an opportunity to tailor the functional materials which are attracted a great attention on their wide range of applications [3–5]. Interestingly, mesoporous materials exhibit wide potential applications in catalysis, sorption, separations, sensing, optics, drug delivery and industrial catalytic reactions, because of their large and uniform pore size with high surface area, multidimensional framework and easy recyclability [6–9]. Moreover, due to high photocatalytic activity, mesoporous materials have successfully been used as photocatalyst for the abatement of pollutants [10–13]. Nevertheless, the use of templates and its high fabrication cost may limit the applications of mesoporous catalysts and may be overcome by developing a simple methodology. However, templates removal needs additional energy and may inhibit the porous structures.

ZnS is one of the important II–VI semiconductor materials with wide band gap energy of 3.5–3.7 eV for cubic zinc blend structure and 3.7–3.8 eV for hexagonal wurtzite structure [14]. In recent years, attention has been focused on heterogeneous photocatalysis for the treatment of recalcitrant and toxic pollutants present in the wastewater [15,16]. Because of its high efficiency, commercial availability and high chemical stability, the photocatalysis is considered one of the most promising remediation processes. Thus, mesoporous photocatalysts offer uniform and adjustable environment for encapsulating the target pollutants on the internal surface of the pores which may increase the degradation rate substantially. Moreover, ZnS was successfully used as a photocatalyst for the degradation of various pollutants under UV light irradiation [17–20]. The modified ZnS was also used as a visible light responsive photocatalyst [4,21,22]. Hu et al. [23], reported a low-cost self-assembly route for the fabrication of nanoporous ZnS and found that the synthesized photocatalysts exhibit superior photocatalytic activity. Therefore, the development of cost-effective, simple and template free, mesoporous photocatalysts with high photocatalytic activity is highly challenge job for scientist.

The fabrication of ZnS microsphere has been reported with and without using templates in various synthetic procedures; however, the synthesis of mesoporous microsphere is limited [24–40]. Thus, in this article, we have reported simple, template free and large

* Corresponding author. Tel.: +358 40 355 3415; fax: +358 15 336 013.
*E-mail addresses:* mmuruganandham@yahoo.com (M. Muruganandham), mika.sillanpaa@lut.fi (M. Sillanpää).

1010-6030/$ – see front matter © 2010 Elsevier B.V. All rights reserved.
doi:10.1016/j.jphotochem.2010.06.008

scale fabrication of mesoporous ZnS with tunable pore size and surface area. The photocatalytic activity of the synthesized photocatalysts was investigated using Methyl Orange dye as a model pollutant. The influence of various experimental parameters on the surface properties and its photocatalytic activity is also reported.

## 2. Experiments

### 2.1. Chemicals

Zinc nitrate hexahydrate, zinc acetate dihydrate, zinc sulfate hepta hydrate, potassium thiocyanate, 2-propanol were obtained from Aldrich chemicals Ltd. (Helsinki, Finland). Methyl Orange (MO) dye was received from Fluka Chemicals Ltd. All these chemicals were used without further purification. For all experimental work Milli Q-Plus water (resistance = 18.2 M Ω) was used.

### 2.2. Synthesis of mesoporous ZnS

In a typical experiment, required amount of $ZnSO_4{\cdot}7H_2O$ is dissolved in 75 mL of water and required amount of potassium thiocyanate is separately dissolved in another 25 mL of water. The molar ratio of $Zn^{2+}$:$SCN^-$ was maintained at 1:2 in all experiments. Under magnetic stirring, potassium thiocyanate was added drop by drop into zinc sulfate solution. The clear solution was stirred for another 30 min and then transferred into a Teflon cup (200 ml) which was covered by a stainless steel cover and the autoclave was kept at 195 °C at desired time in the oven. All other hydrothermal experiments were also performed using the same procedure. After the reaction, the samples were harvested and washed with plenty of water and methanol and finally dried in an oven at 120 °C for few hours. The synthesized catalyst was characterized using appropriate analytical techniques.

### 2.3. Photocatalytic degradation experiment

A 100-mL semibatch reactor, which was made of glass with the dimensions of 6 cm diameter and 10 cm tall, was used to facilitate the operation of all photocatalytic process. The experiments have been performed at room temperature by purging air. In all cases 75 mL of 10 mg/L of Methyl Orange dye solution (natural pH is 5.7) containing 1 g/L mg of the photocatalyst were used. The resulting solution was then stirred continuously in the dark for 30 min to achieve adsorption equilibrium of MO on the photocatalysts. Then, the photocatalytic run was started under UV light (λ = 254 nm) illumination. A low-pressure mercury lamp (Pen-Ray, UVP Inc.) was used for irradiation purpose, which predominantly emits sole wavelength at 254 nm and has an intensity of 5.5 mW/cm$^2$. Samples were withdrawn from the reactor at desired time intervals in the course of the experiments. The solution was filtrated through membrane filter (0.45 μm, polypropylene) in order to remove the catalyst. The absorbance of MO at 463 nm was measured. The absorbance at 463 nm is due to the color of the dye solution and it is used to monitor the decolorization.

### 2.4. Characterization

The X-ray diffraction (XRD) patterns were recorded using a X' Pert PRO PAN analytical diffractometer, scanned angle from 10° to 100°. High resolution transmission electron microscope images were recorded using (FE-TEM, Philips CM-200 FEG - (S) TEM - Super Twin). Samples for HR-TEM were prepared by ultrasonically dispersing the catalyst into ethanol, then placing a drop of this suspension onto a copper grid and then drying in air. The working voltage of TEM was 200 kV. The morphology of the catalyst was examined using a Hitachi S-4100 scanning electron microscope. Prior to SEM measurements, the samples were mounted on a carbon platform which was then coated by platinum using a magnetron sputter for 10 min. The plate containing the sample was then placed in SEM for the analysis with desired magnifications. The surface area, pore size, and pore volume of the catalysts were measured by nitrogen adsorption method using an Autosorp-1 Quantachrome instrument. Prior to analysis, 0.5 g of powder was degassed at 120 °C for 15 h. The X-ray photoelectron spectra were collected on an ESCA-1000 X-ray photoelectron spectrometer (XPS), using Mg Kα X-ray as the excitation source. The UV–visible diffuse reflectance spectra were recorded using a Shimadzu MPS-2000 spectrophotometer and barium sulfate as a standard. The absorbance of the dye was measured using Perkin-Elmer-Lamda-45 spectrophotometer. The percentage of decolourization of MO dye was calculated from the following expressions.

$$\text{Decolourization}\,(\%) = \frac{C_{(\text{MO})0} - C_{(\text{MO})t}}{C_{(\text{MO})0}} \times 100$$

## 3. Results and discussion

The synthesis of zinc sulfide by hydrothermal method was facilitated in aqueous solvent at 195 °C for desired time. One major objective of this research was to prepare mesoporous photocatalysts in large scale and therefore we used higher initial concentration for the synthesis. Initially, we have used 6 g of $Zn^{2+}$ concentration for the synthesis which yields around 10 g of photocatalysts. The formation of zinc sulfide has been confirmed by

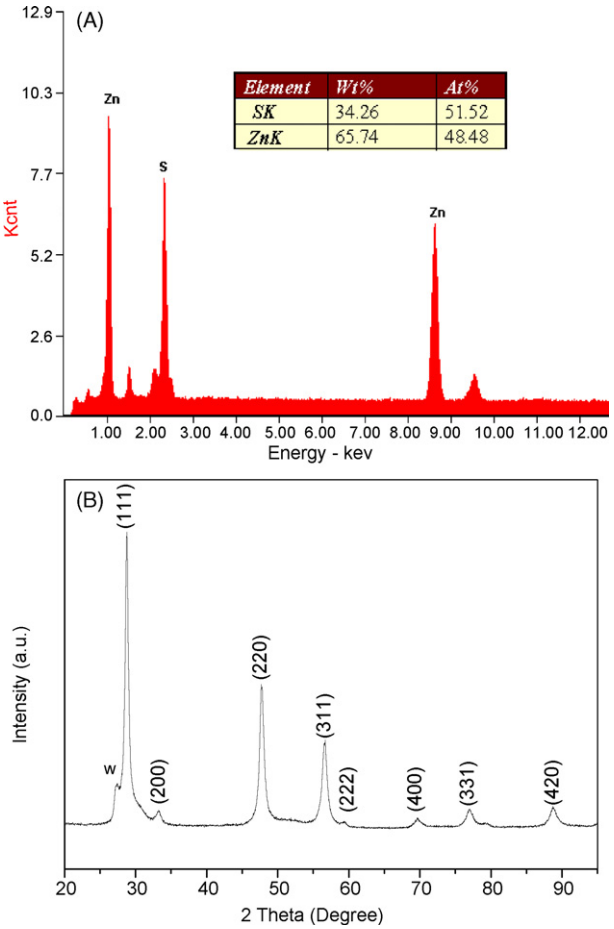


**Fig. 1.** (A) EDX analysis of ZnS and (B) XRD pattern of ZnS.

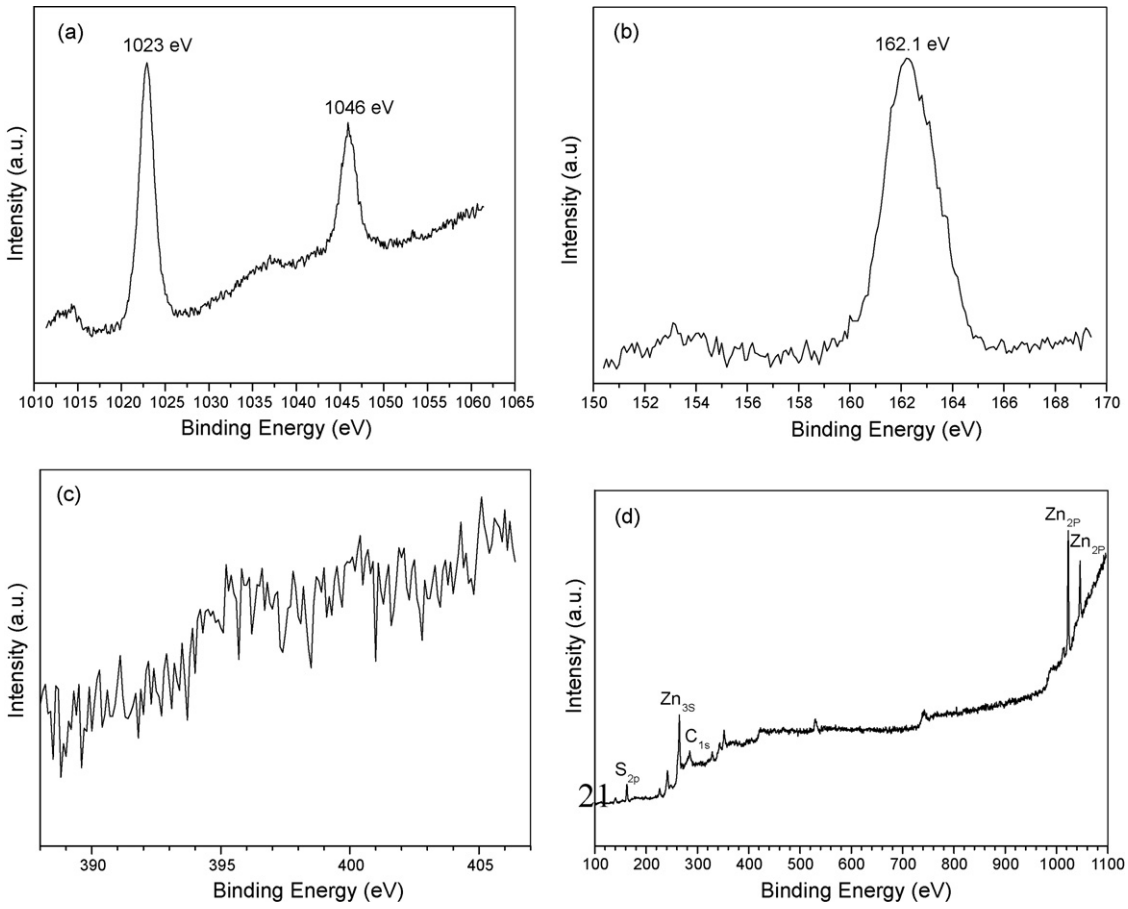


**Fig. 2.** The XPS analysis of ZnS (A) Zn 2p core levels, (B) S 2p core levels, (C) N 1s core levels, and (D) XPS wide survey.

EDX, XRD and XPS analysis. The EDX microanalysis demonstrates that the crystal consists of Zn and S elements and the quantitative analysis confirmed Zn: S ratio nearly equals statiometric ratio (1:1) as shown in Fig. 1A. The XRD pattern in Fig. 1B revels that the synthesized ZnS can be indexed as cubic ZnS (JCPDS card no. 77-2100). However, a peak at 27.3° appears which can be indexed as the (1 0 0) reflection of hexagonal wurtzite phase. The percentage of hexagonal phase is less when compared to cubic phase. No other impurities

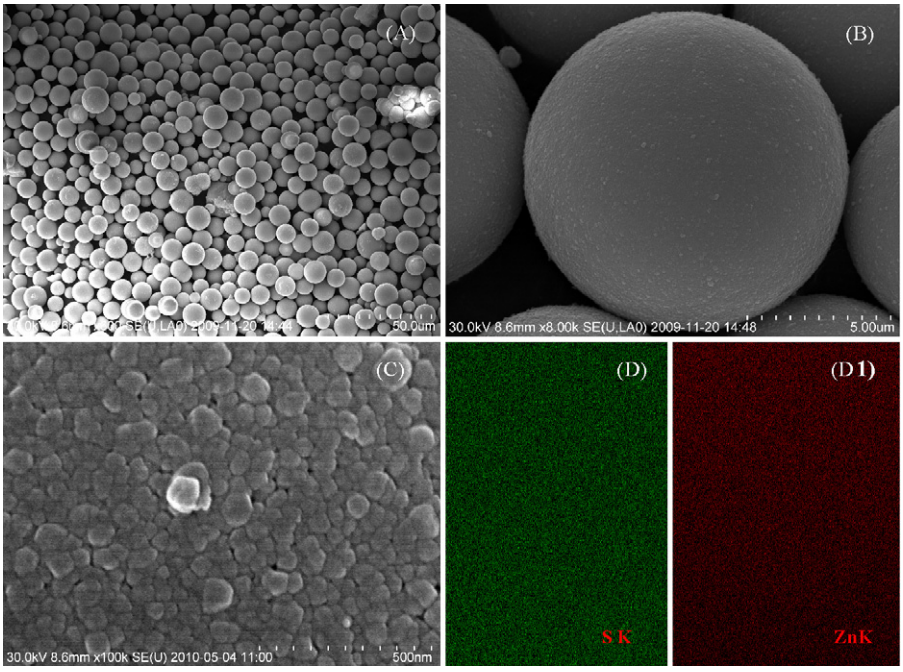


**Fig. 3.** The FE-SEM pictures (A–C) and (D) elemental mapping of zinc and sulfur atom of synthesized ZnS.

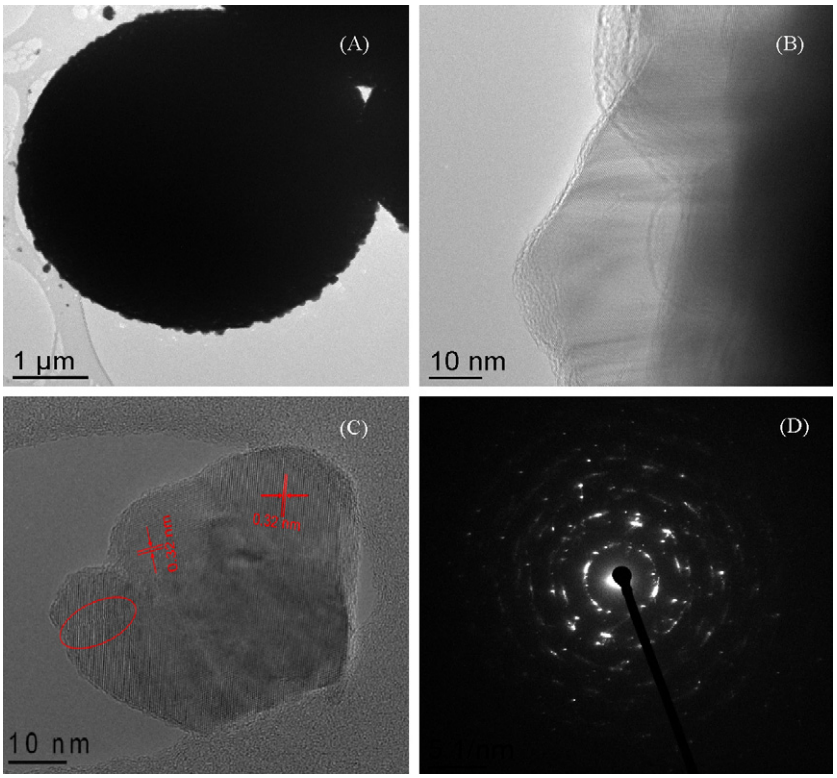


**Fig. 4.** The HR-TEM images ZnS (A) microsphere, (B and C) lattice fringes and (D) SAED pattern.

peaks were noted in XRD which imply the formation pure ZnS. In order to confirm the chemical purity of synthesized ZnS, the XPS analysis was studied and the results are presented in Fig. 2. The XPS Zn $2p_{3/2}$ and Zn $2p_{1/2}$ peaks found at 1023 and 1046 eV indicated that zinc presented as zinc sulfide. Similarly, the S 2p peak found at 162.5 eV which implies that sulfur exists as sulfides. No additional peaks were observed from 165 to 170 eV, which clearly demonstrated the absence of an oxidized form of sulfur. The XPS spectra also confirm the absence of possible impurities like K, N and C which indicated the purity of the synthesized photocatalyst as confirmed in Fig. 2C and D. However, a weak O1S XPS peak was noted and based on further analyses; we found that the O peak comes from air and such impurities peak were noted in other samples during XPS analysis.

The FE-SEM pictures showed in Fig. 3A and B confirms the formation of microsphere. It is quite interesting to note that the formed microspheres were aggregates free, well dispersed, and its surface structures are uniform with size ranging from 1 to 5 μm. The high magnification FE-SEM picture in Fig. 3C showed that the microsphere surface was assembled by small nanoparticles size ranging from 5 to 15 nm. The elemental mapping of both zinc and sulfur showed homogeneous distribution as shown in Fig. 3D. Due to the large size of the microsphere (Fig. 4A), the HR-TEM analysis provided only limited information. We were not able to analyze the surface of the microspheres and therefore analysis was done on the edge of the microspheres. Thus, close examination of the microsphere reveals that the microspheres formed by small nanoparticles which were assembled by oriented attachment as confirmed by Fig. 4B. The nanoparticles lattice fringes in Fig. 4C reveals a part of well crystallized and amorphous nature of the catalysts. The SAED pattern implies polycrystalline nature of the microspheres (Fig. 4D).

Fig. 5 shows a typical $N_2$ gas adsorption–desorption isotherm. The isotherm displays the typical type IV curve, which is usually attributed to the predominance of mesopores. The high magnifica-

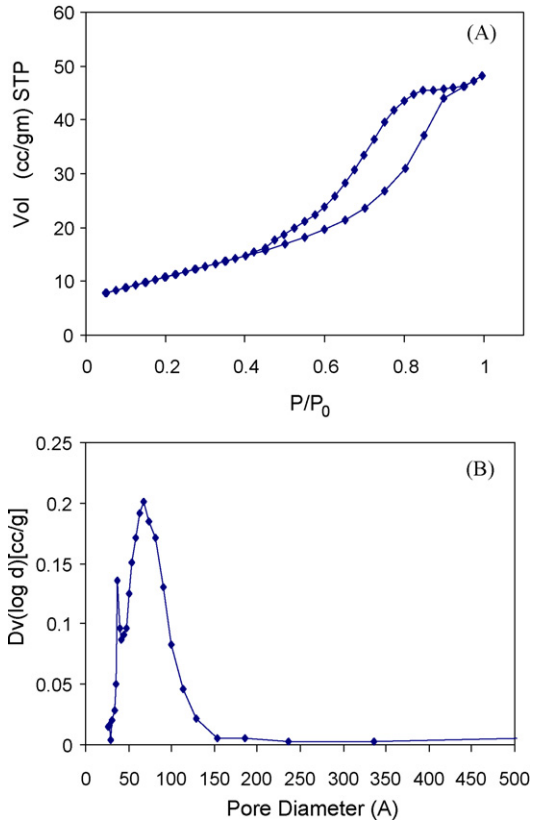


**Fig. 5.** The nitrogen adsorption analysis of ZnS prepared at 195 °C for 10 h (A). The nitrogen adsorption–desorption analysis results (B) pore size distribution.

tion FE-SEM picture (Fig. 3C) shows that the mesopores are formed between the particles on the microsphere surface. The average pore size and pore volume was found to be 7.2 nm and 0.052 cc/g, respectively. The BET surface area was found to be 40 $m^2$/g. The noted surface area is higher than the mesoporous ZnS nanospheres reported in the literature [41]. The narrow pore size indicated uniform pore size distribution on the microspheres surface. Therefore, this synthetic methodology open a door to synthesis precisely controlled, mesopore structured, uniform ZnS microsphere.

### 3.1. Influence of experimental parameters on the morphology and surface properties

Generally, various surface properties of the photocatalyst played important role to control the efficiency of photocatalysts. Therefore, in order to prepare highly active photocatalyst and to understand the influence of various experimental parameters on the formation of mesoporous ZnS microsphere, the synthesis has been studied under different experimental conditions. For examples, Yu et al. [41], synthesized solid microspheres using zinc salt and thiourea with 1.6 and 40 mmol in a hydrothermal process. However, Jayalakshmi and Mohan Rao [42], prepared zinc sulfide nanoparticles using 1:1 molar ratio of zinc salt with thiourea. The aforementioned results clearly explain the importance of experimental parameters on the synthesized materials. Therefore, it is interesting to study the influence of initial concentration of the precursors, various zinc precursors, hydrothermal reaction time and temperature.

The formation of ZnS microsphere was investigated using zinc sulfate, zinc nitrate and zinc acetate as zinc precursor while keeping KSCN as thiocyanate source. The hydrothermal synthesis was carried out using 4 g of $Zn^{2+}$ initial concentration at 195 °C for 10 h. The XRD results in Fig. 6 confirmed the formation of cubic phase ZnS from all three zinc precursors. As discussed earlier, the wurtzite phase peak coexists along with (1 1 1) peak of the cubic phase and wurtzite phase is noted in all three synthesized samples. Fig. 7 shows the formation of two different types of microspheres. Though, zinc sulfate and zinc nitrate facilitates microsphere, zinc acetate yields flower like morphology. Nevertheless, high magnification FE-SEM clearly shows that both microspheres and microflowers surface were assembled by nanoparticles. Thus, such self-assembly of nanoparticles may result mesoporous surface structures in both morphology. The formation of mesoporous structure from zinc sulfate at higher initial concentration (6 g of $Zn^{2+}$) was already presented in Fig. 5. Zinc sulfate also facilitated mesoporous structure at low concentration (4 g of $Zn^{2+}$) and the results are presented in Fig. 10A. In order to confirm the formation of mesoporous structured ZnS from other zinc precursors, the microspheres formed from zinc acetate was examined. The nitrogen adsorption experiments confirm the formation of mesoporous ZnS with the average pore size of 3.7 nm. These experimental results revels that the zinc precursor did not influence the formation of mesoporous surface structure.

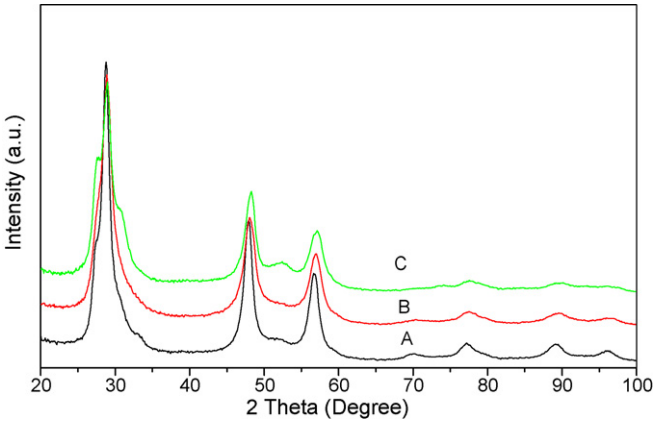


**Fig. 6.** The XRD pattern of ZnS prepared using (A) zinc sulfate, (B) zinc acetate, and (C) zinc nitrate.

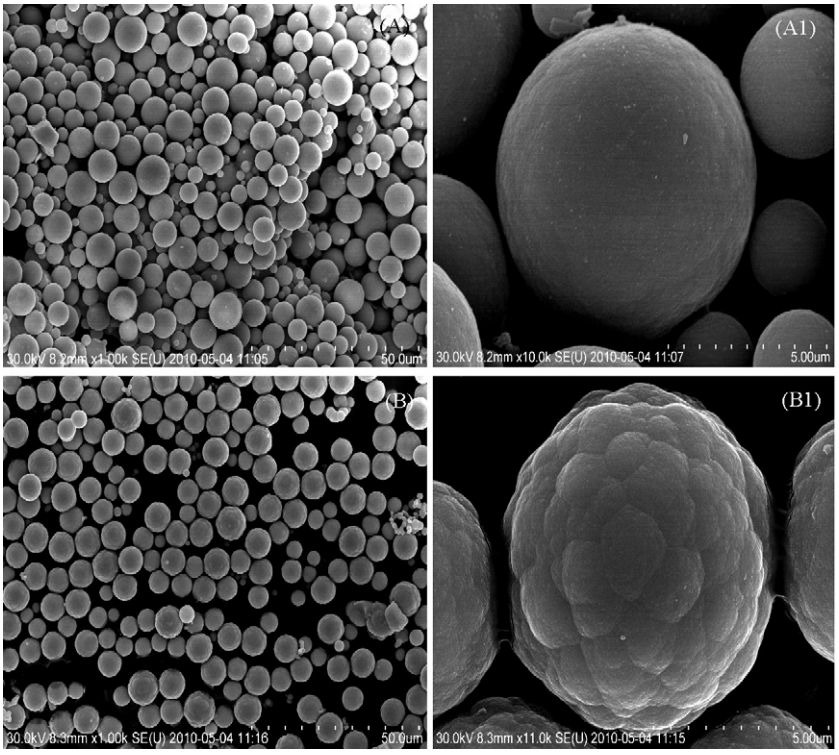


**Fig. 7.** The FE-SEM pictures of ZnS prepared at 195 °C for 10 h using (A) zinc nitrate and (B) zinc acetate.

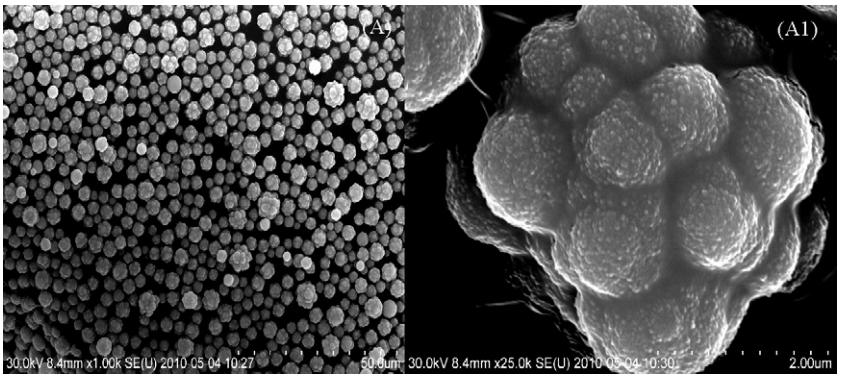


**Fig. 8.** FE-SEM pictures of ZnS prepared using 0.6 g of $Zn^{2+}$ initial concentration at 195 °C for 10 h.

The influence of initial concentration of the precursor was investigated by changing the initial concentration of $Zn^{2+}$ from 6 to 0.6 g and the results are shown in Fig. 8. The FE-SEM picture clearly indicated that low concentration of the precursor (0.6 g) results flowerlike morphology and are almost similar to one formed in zinc acetate as precursor. However, further increase the concentration results quite similar morphology presented in Fig. 3B. Though, the morphology is different, all ZnS posses quite similar surface structure i.e. self-assembled by nanoparticles. Interestingly, the noted pore size of the microsphere is varying according to the concentration of the precursors. The average pore size of 2.6, 3.4 and 7.5 nm and 39, 64 and 40 $m^2$/g, is noted when the initial concentration of 0.6, 4 and 6 g of $Zn^{2+}$, respectively. These results indicated that by simply adjusting the precursor concentration we could control the pore size. However, higher pore volume (0.74 cc/g) is noted at higher initial concentration (6 g) when compared to other two concentrations which yield 0.52 cc/g. Moreover, such precisely controlled, narrow pore size, pore tunable synthesis is the novelty of this research and such self-assembly is not reported earlier. Sun et al. [43], reported co-template approach for the pore size enlargement of mesoporous ZnS and such fabrication involves complicated procedures.

One of the important experimental parameters that influenced the formation of ZnS is hydrothermal temperature. Unlike, other sulfur sources like thiourea and thioacetamide; thiocyanate complex facilitates ZnS only at higher temperatures. As evident from hydrothermal experiments, at low temperature (140 °C), the ZnS is formed after 24 h and even after 48 h the yield of ZnS is very low. Therefore, all hydrothermal reaction was studied at 195 °C. The time dependent morphological evaluation and surface properties were investigated at 3, 6 and 10 h at 195 °C and the results are presented in Fig. 9. The FE-SEM pictures confirmed the formation of microsphere at all reaction time, however, a notable difference observed in the microsphere size. After 3 and 6 h nanospheres with size ranging from 400 nm to 1 μm were also noted with microspheres and such nanospheres were not observed after 10 h. These results confirm the involvement of Ostwald ripening process during the microspheres formation. The surface properties of the microsphere formed at different reaction times were studied. The BET surface area and the average pore size of the microspheres were found to be 74, 63, and 74 $m^2$/g and 2.6, 3.2, and 3.4 nm after 3, 6 and 10 h, respectively. A representative nitrogen adsorption analysis result of ZnS prepared after 6 h is presented in Fig. 10B. The higher surface area at early stages of the hydrothermal process is

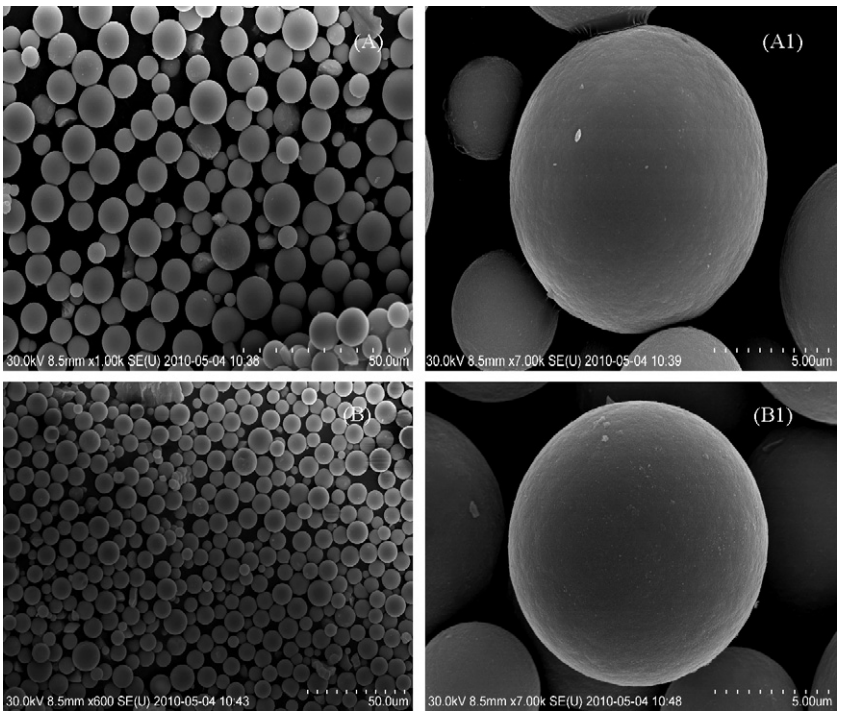


**Fig. 9.** The FE-SEM pictures of ZnS prepared at 195 °C for (A) 3 h and (B) 6 h.

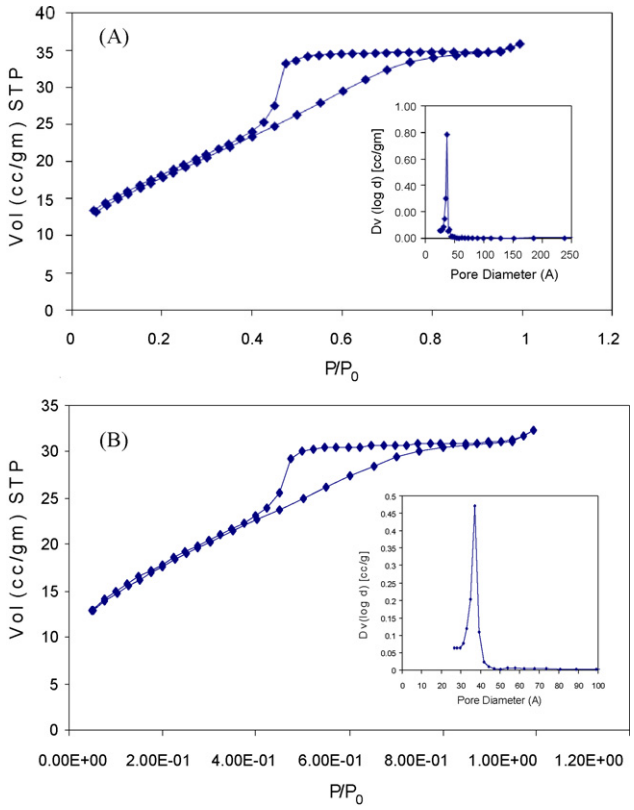


**Fig. 10.** The nitrogen adsorption analysis ZnS prepared using 4 g of $Zn^{2+}$ initial concentration at 195 °C for (A) 10 h and (B) 6 h.

mainly due to the difference in the size of the microspheres at different reaction times. However, there is no obvious change on the surface properties of microspheres when the hydrothermal reaction time increases from 6 to 10 h. Generally, the particles sizes are also one of the influencing parameters for the surface area of the mesoporous materials. Sun et al. [43], synthesized mesoporous ZnS nanoparticles with the surface area of 354 $m^2\,g^{-1}$ and similar high surface area is not observed in microsize ZnS reported in the literatures. In conclusion, the surface area of the synthesized ZnS photocatalysts is influenced by the size of the microspheres.

### 3.2. Mechanism

The thiocyanate ion can bind to metal ions through either the S or N atom [44]. In principle, zinc (II) is a borderline element of hard and soft acids. As the thiocyanate ion possesses two different donor atoms of the softer S and the harder N, and the zinc (II) ion certainly is a hard acceptor and coordinates via N to form the tetrahedral coordination complex [45]. Thus, it is expected that the zinc ion coordinates with nitrogen, which results in a $[Zn(NCS)_2]$ complex in water. We have successfully synthesized N, C co-doped hierarchical porous ZnS by thermal decomposition of zinc isothiocyanate complex in air [4]. The formation of microsphere is also investigated using other sulfur sources such as thiourea and thioacetamide under similar experimental conditions. The results clearly shows that thiourea and thiocyanate facilitates microsphere formation, where as thioacetamide facilitates nanoplate like particles. The hydrothermal process results in weakening of the coordination of the Zn-NCS complex and $Zn^{2+}$ will be released gradually. Meanwhile, the C=S and C=N double bonds of thiocyanate will be broken to release $S^{2-}$ anions. Then the active $S^{2-}$ reacts with $Zn^{2+}$ to generate the ZnS nuclei. The formation of microspheres after fast nucleation is mainly related to two primary mechanisms:

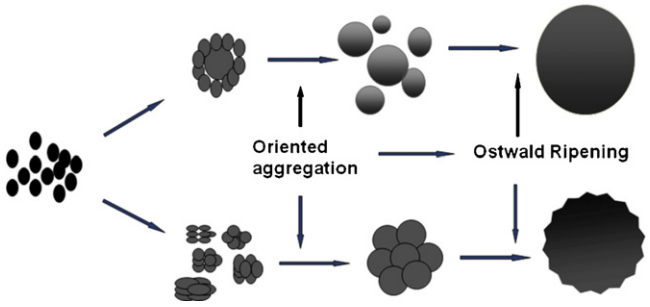


**Scheme 1.** The schematic formation of microspheres and microflowers.

random aggregation and Ostwald ripening. At this initial stage, most of the primary spherical aggregates were inclined to capture the monomers in the solution to form larger ones due to the high concentration of the monomer. Driven by the minimization of interfacial energy, the initially formed nanocrystals would act as primary building blocks to produce larger self-assembled aggregates. Thus, such aggregation facilitated by oriented attachment of nanoparticles as evident from HR-TEM image as shown in Fig. 4B. Subsequently, due to the polydispersity of the nanoparticles, Ostwald ripening occurred in small spherical aggregates because the smaller particles have a higher surface energy and are hence less stable than larger ones which tend to dissolve and recrystallize on larger ones. This kind of attachment process is thermodynamically favorable, since the surface energy is significantly reduced due to the elimination of the interface [46]. These loosely bound microspheres undergo restructuring or rearranging into a more compact/dense microsphere texture. The process repeated continuously until the disappearance of all small particles and only the perfect microsphere structure was appeared as shown in the time dependent FE-SEM pictures. The corresponding SAED pattern depicts that the sphere is polycrystalline in nature because the sphere is composed of numerous nanocrystals. Generally, additives are necessary for the oriented aggregation-based self-assembly in solution system. As no additives were added in our synthesis we believe that the Ostwald ripening is more suitable to explain the mechanism. In addition to the above discussed mechanism, the flower shaped microparticles formed when we use zinc acetate instead of zinc sulfate and this may be due to the by-products formed in the hydrothermal process could influence the crystal growth. However, we do not have enough evidence to support our speculation and further multifold analysis is necessary to understand clearly and will be addressed in our future publication. The schematic formation mechanism of microsphere is shown in Scheme 1.

### 3.3. Photocatalytic evaluation of mesoporous ZnS

It is known that many properties of the photocatalysts such as crystalline phase, size, morphology, specific surface area, and defect, can affect its photocatalytic activity. Therefore, it is very interesting to study the photocatalytic activity of mesoporous ZnS prepared under different experimental conditions. The photocatalytic activity was evaluated using MO dye as a model pollutant under UV light irradiation and the efficiency was compared with commercially available ZnS. The UV–visible diffuse reflectance spectra showed absorption wavelength in the UV region as shown in Fig. 11. The DRS spectra of other samples also similar to one displayed in Fig. 11 and therefore synthesized conditions could not affect the absorbance spectra of ZnS. The onset absorption wavelength and corresponding band gap were found to be 390 and 3.17 eV, respectively. The controlled experiments showed that 1 g/L of photocatalysts was found to be optimum for efficient degra-

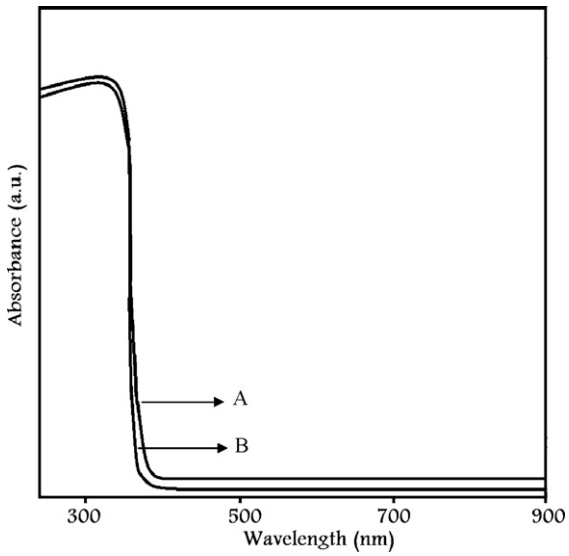


**Fig. 11.** DRS spectra of ZnS (A) synthesized ZnS and (B) commercial ZnS.

dation and therefore all experiments were performed using 1 g/L at natural pH. Initially, the photocatalytic activity was studied with the photocatalyst prepared using various zinc precursors. Fig. 12A shows the photocatalytic decolourization results using three different photocatalysts prepared under similar experimental conditions. About 77, 63.1 and 58% of decolurization is noted after 30 min of irradiation with the photocatalysts prepared using zinc sulfate, zinc acetate and zinc nitrate, respectively. The degradation efficiency of the mentioned photocatalysts is in good agreement with the surface properties of the photocatalysts. Despite, similar

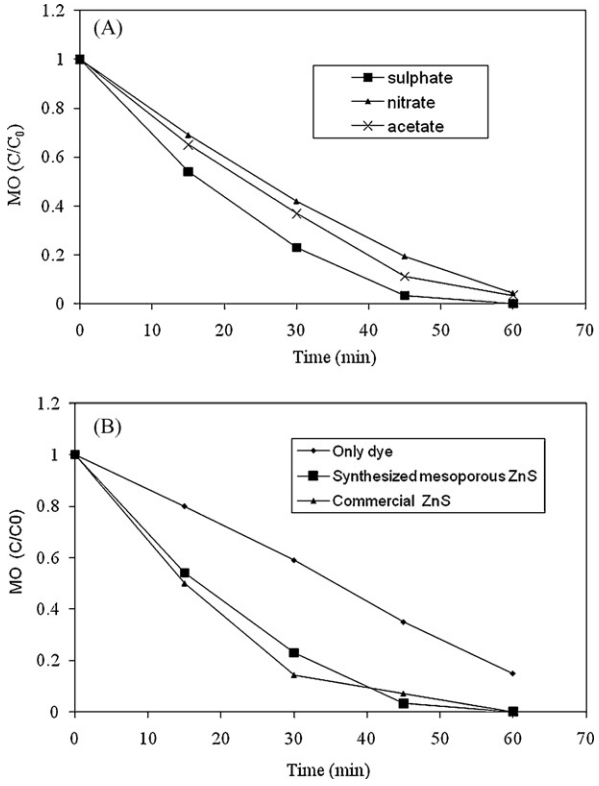


**Fig. 12.** Photocatalytic decolourization of MO dye in the presence of mesoporous ZnS prepared using (A) various zinc precursors and (B) under different experimental conditions. [Catalysts] = 1 g/L, [MO] = 10 mg/L, pH = 5.7, temperature = 25 °C.

pore size and pore volume of these three photocatalysts, the surface area of the photocatalysts prepared using zinc sulfate is higher than other two catalyst which may result in higher photocatalytic activity. In order to understand the influence of hydrothermal reaction time on the photocatalytic activity, photocatalytic degradation experiments were performed with photocatalysts prepared after 3 and 10 h. The surface area of the above mentioned mesoporous photocatalysts are 74 and 64 $m^2$/g. The decolourization results in Fig. 12B confirm that the photocatalysts prepared at 10 h has higher photocatalytic activity than prepared at 3 h. Despite low surface area the photocatalysts prepared at 10 h, it showed better photocatalytic efficiency and this may be due to the difference in the crystallization of the two photocatalysts. The XRD results of these two samples showed that the photocatalysts prepared at 10 h is well crystallized when compared to one prepared at 3 h. In order to understand the influence of crystallization effect, additional experiments were also performed. Thus, the photocatalytic activity of commercially available cubic phase ZnS was investigated and the photocatalysts is well crystallized (confirmed by XRD), low surface area (16 $m^2$/g). This photocatalyst is ideal candidate to confirm the influence of crystallization effect on the photocatalytic activity with synthesized mesoporous photocatalysts. The photocatalytic decolourization experiments showed that the efficiency of commercial catalysts is almost equals to the synthesized mesoporous photocatalysts (10 h), despite low surface area of the photocatalysts and the results are presented in Fig. 12B. The high efficiency is due to well crystalline nature of the commercial sample. In conclusion, well crystallized and high surface photocatalyst yields high photocatalytic activity.

To understand the active species involved in the photocatalytic process, the formation of hydroxyl radicals were confirmed in the photocatalytic process. The •OH radical rate constant with 2-propanol is $3.1 \times 10^9$ L/(mol S) [47]. About 58 and 60% of degradation was noted in the presence 100 and 250 μl of 2-propanol whereas in the absence of 2-propanol 77% of decolourization were noted. The decrease in degradation rate in the presence of 2-propanol is due to hydroxyl scavenging effect which decrease the availability of hydroxyl radical for dye degradation. These results clearly confirm the generation of hydroxyl radical in the photocatalytic degradation process.

### 3.4. Catalytic reusability and recyclability

One of the main disadvantages of slurry type photocatalytic process is separation of photocatalysts after its task in the treatment process. Therefore, the photocatalyst is expected to be reclaimed by a simple method. Since the catalytic stability and reusability are important factors in catalyzed reactions, it is necessary to study the stability of the used catalyst. If the stability is poor or deactivation of the catalyst is severe, the catalyst will be useless in a practical industrial application. It is known that sulfide photocatalysts such as ZnS may undergo photocorrosive oxidation during the photocatalytic degradation process which results sulfate ions [48,49]. The entire catalytic reusability test has been investigated under identical reaction conditions. To evaluate the catalytic reusability, we have studied the photocatalytic activity in three consecutive cycles. The results indicated (not presented in the figure) that the photocatalyst retains its photocatalytic activity in three cycles. These results imply that the mesoporous ZnS photocatalysts can be used for long term environmental remediation process.

The catalytic recyclability of the mesoporous microsphere has been studied and compared with commercially available ZnS and $TiO_2$ photocatalysts. About 0.025 g of the microsphere catalysts was suspended in 7 mL of water and ultrasonicated for 5 min, and the separation was noted after 5 min, as shown in Fig. 13. Obviously, synthesized microsphere (A) is quite easily separated in a short time

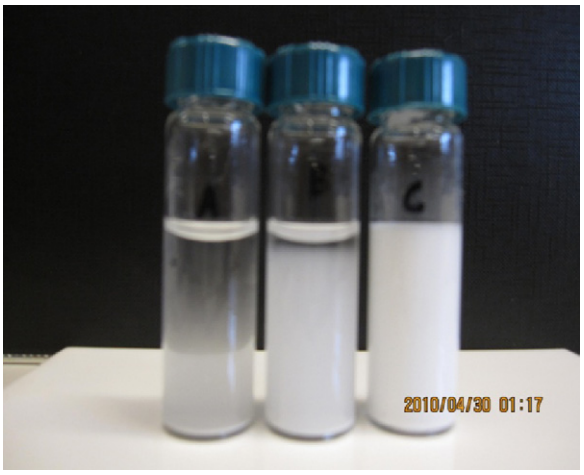


**Fig. 13.** Catalytic recyclability of [A] = ZnS microspheres, [B] = ZnS nanoparticles, and [C] = $TiO_2$ nanoparticles.

as compared to commercial ZnS (B) and $TiO_2$ (C) colloids which indicates that the ZnS microsphere is easily recyclable photocatalysts. Similar observation is also noted in other easily recyclable photocatalyst [50,51]. In conclusion, mesoporous ZnS microsphere is a highly efficient and easily recyclable photocatalyst.

## 4. Conclusions

We have successfully synthesized mono dispersed, aggregates free, homogenous surface structured mesoporous ZnS microsphere by self-assembled process without using template or catalysts in large scale. By simply adjusting the experimental parameters, we could tune the pore size, pore volume and surface area of the photocatalysts. The XRD pattern reveals the formation of cubic phase ZnS with small percentages of wurtzite phase. Despite, the difference in the morphology of the synthesized photocatalyst, the microspheres surface was assembled by nanoparticles by oriented attachment and mesopores are formed in between the nanoparticles. The photocatalytic degradation experiments showed that well crystallized, high surface area photocatalyst yields higher photocatalytic activity. The hydroxyl radical is the main oxidizing species in the photodegradation process. The photocatalytic reusability was investigated up to three successive cycles and found that the catalytic retains its activity even after three cycles. The catalytic recyclability experiments showed that mesoporous ZnS microspheres are easily recyclable when compared to commercial ZnS and $TiO_2$.

## Acknowledgment

M.M. gratefully acknowledges EU Transfer of Knowledge Marie Curie grants MKTD-CT-2006-042637.

## References

[1] Y.D. Yin, A.P. Alivisatos, Nature 437 (2005) 664–670.
[2] Y. Sun, Y. Xia, Science 298 (2002) 2176–2179.
[3] Z.M. Fresco, M.J. Frechet, J. Am. Chem. Soc. 127 (2005) 8302–8303.
[4] M. Muruganandham, Y. Kusumoto, J. Phys. Chem. C 113 (2009) 16144–16150.
[5] B. Yan, H.-F. Lu, J. Photochem. Photobiol. A: Chem. 205 (2009) 122–128.
[6] J. Yu, H. Yu, B. Cheng, X. Zhao, Q. Zhang, J. Photochem. Photobiol. A: Chem. 182 (2006) 121–127.
[7] Y. Ren, A.R. Armstrong, F. Jiao, P.G. Bruce, J. Am. Chem. Soc. 132 (2010) 996–1004.
[8] H. Lin, G. Zhu, J. Xing, B. Gao, S. Qiu, Langmuir 25 (2009) 10159–10164.
[9] B. Yan, B. Zhou, J. Photochem. Photobiol. A: Chem. 195 (2008) 314–322.
[10] J.S. Jang, C.-J. Yu, S.H. Choi, S.M. Ji, E.S. Kim, J.S. Lee, J. Catal. 254 (2008) 144–155.
[11] X. Wang, J.C. Yu, Y. Hou, X. Fu, Adv. Mater. 17 (2005) 99–102.
[12] H. Wang, Z. Wu, Y. Liu, J. Phys. Chem. C 113 (2009) 13317–13324.
[13] J. Yu, W. Wang, B. Cheng, B.-L. Su, J. Phys. Chem. C 113 (2009) 6743–6750.
[14] B.Y. Geng, X.W. Liu, Q.B. Du, X.W. Wei, L.D. Zhang, Appl. Phys. Lett. 88 (2006) 163104.
[15] S. Vilhunen, M. Bosund, M.-L. Kääriäinen, D. Cameron, M. Sillanpää, Sep. Purif. Technol. 66 (2009) 130–134.
[16] K. Pirkanniemi, M. Sillanpää, Chemosphere 48 (2002) 1047–1060.
[17] H. Yin, Y. Wada, T. Kitamura, H. Yanagida, Environ. Sci. Technol. 35 (2001) 227–231.
[18] Q. Zhao, Y. Xie, Z. Zhang, X. Bai, Cryst. Growth Des. 7 (2007) 153–158.
[19] M. El-Kemary, H. El-Shamy, J. Photochem. Photobiol. A: Chem. 205 (2009) 151–155.
[20] J.S. Jang, C.-J. Yu, S.-H. Choi, S.M. Ji, E.S. Kim, J.S. Lee, J. Catal. 254 (2008) 144–155.
[21] T. Arai, S. Senda, Y. Sato, H. Takahashi, K. Shinoda, B. Jeyadevan, K. Tohji, Chem. Mater. 20 (2008) 1997–2000.
[22] I. Tsuji, A. Kudo, J. Photochem. Photobiol. A: Chem. 156 (2003) 249–252.
[23] J.S. Hu, L.L. Ren, Y.G. Guo, H.P. Liang, A.M. Cao, L.J. Wan, C.L. Bai, Angew. Chem. Int. Ed. 44 (2005) 1269.
[24] A. Wolosiuk, O. Armagan, P.V. Braun, J. Am. Chem. Soc. 127 (2005) 16356–16357.
[25] C. Yan, D. Xue, J. Phys. Chem. B 110 (2006) 7102–7106.
[26] H. Tong, Y.-J. Zhu, L.-X. Yang, L. Li, L. Zhang, J. Chang, L.-Q. An, S.-W. Wang, J. Phys. Chem. C 111 (2007) 3893–3900.
[27] Y. Luo, G. Duan, M. Ye, Y. Zhang, G. Li, J. Phys. Chem. C 112 (2008) 2349–2352.
[28] Y. Ma, L. Qi, J. Ma, H. Cheng, Langmuir 19 (2003) 4040–4042.
[29] Y.F. Zhu, D.H. Fan, W.Z. Shen, Langmuir 24 (2008) 11131–11136.
[30] H. Zhou, T. Fan, D. Zhang, Q. Guo, H. Ogawa, Chem. Mater. 19 (2007) 2144–2146.
[31] Q. Wu, H. Cao, S. Zhang, X. Zhang, Inorg. Chem. 45 (2006) 4586–4588.
[32] Q. Wu, H. Cao, S. Zhang, X. Zhang, R. Daniel, Inorg. Chem. 45 (2006) 7316–7322.
[33] Q.-Z. Yao, G. Jin, G.-T. Zhou, Mater. Chem. Phys. 109 (2008) 164–168.
[34] L. Yang, J. Han, T. Luo, M. Li, J. Huang, F. Meng, J. Liu, Asian Chem. J. 4 (2009) 174–180.
[35] Z. Pi, X. Su, C. Yang, X. Tian, F. Pei, S. Zhang, J. Zheng, Mater. Res. Bull. 43 (2008) 1966–1970.
[36] Y. He, Mater. Res. Bull. 40 (2005) 629–634.
[37] X. Liu, J. Cui, L. Zhang, W. Yu, F. Guo, Y. Qian, Mater. Lett. 60 (2006) 2465–2469.
[38] C. Jiang, W. Zhang, G. Zou, W. Yu, Y. Qian, Mater. Chem. Phys. 103 (2007) 24–27.
[39] Y. Zhao, W. Shi, M. Gong, F. Yu, T. Chen, Mater. Chem. Phys. 94 (2005) 292–297.
[40] X. Wang, F. Wan, K. Han, C. Chai, K. Jiang, Mater. Charact. 59 (2008) 1765–1770.
[41] X. Yu, J. Yu, B. Cheng, B. Huang, Chem. Eur. J. 15 (2009) 6731–6739.
[42] M. Jayalakshmi, M. Mohan Rao, J. Power Sources 157 (2006) 624–629.
[43] Z.-X. Sun, Q. Zhang, Y.-H. Lu, Y.-L. Li, Micropor. Mesopor. Mater. 109 (2008) 376–382.
[44] T. Yamaguchi, K. Yamamoto, H. Ohtaki, Bull. Chem. Soc. Jpn. 58 (1985) 3235–3241.
[45] S. Ahrland, L. Kullberg, Acta Chem. Scand. 25 (1971) 3692–3704.
[46] J.F. Banfield, S.A. Welch, H. Zhang, T.T. Ebert, R.L. Penn, Science 289 (2000) 751–754.
[47] J.J. Wu, J.-S. Yang, M. Muruganandham, Ind. Eng. Chem. Res. 47 (2008) 1820–1827.
[48] J.-F. Reber, K.J. Meier, Phys. Chem. 88 (1984) 5903–5913.
[49] D. Meissner, R. Memming, B. Kastening, J. Phys. Chem. 92 (1988) 3476–3483.
[50] M. Muruganandham, J.J. Wu, Appl. Catal. B: Environ. 80 (2008) 32–41.
[51] M. Muruganandham, Y. Kusumoto, C. Okamoto, M. Amutha, Md. Mamun, A. Bashir, J. Phys. Chem. C 113 (2009) 19506–19517.